

Anisotropy of flexible polymers and one-dimensional Brownian motion

Guillermo Narvaez Paliza¹

¹*Martin A. Fisher School of Physics, Brandeis University, Waltham, MA 02453, USA*

(Dated: April 2, 2017)

In the microscopic world, physical systems are significantly more sensitive to individual interactions than macroscopic ones. Microparticles tend to follow a diffusive motion rather than a ballistic motion, making it harder to predict the dynamics of a system. Here we explore the validity of using computer simulations to substitute real physical systems and predict their dynamical properties using mathematical and probabilistic tools. We explore flexible polymers in solution and particles undergoing Brownian motion in a one-dimensional medium and show that the systems can be safely approximated by numerical methods involving the generation of random numbers. We show that the anisotropy of flexible polymers' shapes is mostly due to the random walk nature of the system and not due to intramolecular interactions or self-avoiding effects. We show that the Langevine equation can be used to predict the trajectory of a Brownian particle while ignoring the inertial term, and that a Monte Carlo algorithm can be used to describe more precisely and at a cheaper cost the properties of an equilibrated system.

INTRODUCTION

Often when studying macroscopic systems their behavior is, within a certain degree of uncertainty, defined by a ballistic motion. We can use equations to understand and accurately predict the motion of a projectile. However, when we look into the microscopic world, these ballistic tools seem useless. At the very small scale, physical systems tend to be characterized by a diffusive motion. At the small scale, every small interaction becomes significant and the sum of all interactions adds up to a seemingly random movement. In 1905, Karl Pearson introduced the term *random walk*. A random walk is a mathematical tool used to approximate or simulate diffusive motion. It is the continuous unitary displacement in random directions. In this paper we exploit this mathematical tool in order to explore the random walk nature of flexible polymers and particles in Brownian motion.

Our approach involves writing computer programs that simulate two interesting systems. The first one, a flexible polymer in solution, the second one, a spherical particle undergoing Brownian motion in one dimension. The simulations explore the dynamics of the system and are compared to the literature. Each of these physical systems is treated separately. Our objective, however, is in both cases to qualitatively explore the correlation between a mathematical tool, random walks, and a real physical system. By comparing statistical information from the simulations to experimental results we can determine the extent of the influence of random walks in our microscopic systems.

RANDOM WALKS IN FLEXIBLE POLYMERS

A random walk displacement is characterized by its squared mean displacement being proportional to the square root of the number of steps, $\langle x^2 \rangle \propto \sqrt{N}$, where N

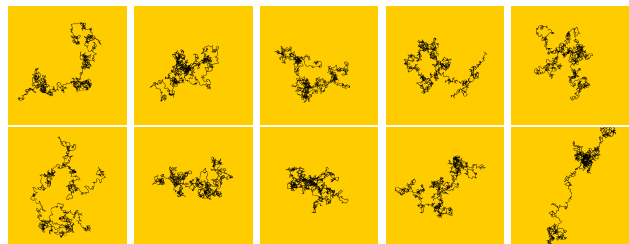


FIG. 1: Simulation results for 10 flexible polymers consisting of 1000 monomers each. The simulations are completely dependent on a pseudo-random generator.

The polymers exist in a two-dimensional space.

is the number of steps. We shall see this relationship later on on the characterization of the polymers. In generating polymers of length N , we generate a random number θ_i , where $0 \leq \theta_i \leq 2\pi$ for the i -th monomer, and use the following expression sequentially

$$\mathbf{r}_N = \mathbf{r}_i + \sum_{i=2}^N (\cos \theta_i, \sin \theta_i) \quad (1)$$

We generated 10 polymers, each of $N = 1000$. From Figure 1 we can observe that the polymers' shapes differ significantly from one to the other. However, we can see that the polymers do not obey a spherical symmetry, but their shapes are anisotropic. We can also see that the length of the polymer is significantly smaller than the length of N monomers aligned as a rod (about 10% of the possible maximum length).

In order to characterize the shape of the polymers we define three different measures of the polymer. The end-to-end radius consists of the distance between the first and last monomers of the polymer,

$$R_{ee} \equiv |\mathbf{r}_N - \mathbf{r}_1| \quad (2)$$

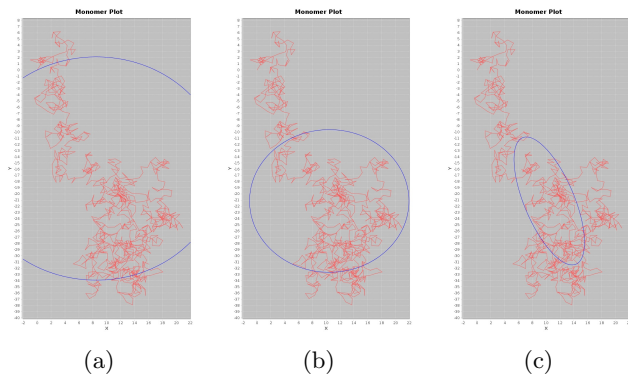


FIG. 2: A particular polymer of length 1000 monomers, plotted with its different shape characterizations. (a) The end-to-end circle, (b) the gyration circle, and (c) the gaussian ellipse.

The gyration radius is a more general measure of the spread of the polymer, defined as

$$R_g^2 = \sum_{i=1}^N |\mathbf{r}_N - \mathbf{r}_1|^2 / N \quad (3)$$

The last characterization is the gaussian ellipse of the polymer. The two radii and the orientation of the polymer are extracted from the covariance tensor

$$V \equiv \sum_{i=1}^N \frac{1}{N} \begin{bmatrix} (x_i - \bar{x})^2 & (x_i - \bar{x})(y_i - \bar{y}) \\ (x_i - \bar{x})(y_i - \bar{y}) & (y_i - \bar{y})^2 \end{bmatrix} \quad (4)$$

where the eigenvectors of the matrix represent the orientations of the major and minor axis of the ellipse, and the eigenvalues are α^2 and β^2 . The major radius of the gaussian ellipse is α and the minor radius is β . We will characterize the orientation of the polymer Θ , as $\Theta \equiv \arccos \alpha_x$.

It is clear from the polymer's shape characterizations showed in Figure 2 for a particular flexible polymer that the shape characterizations do not offer enough insight by themselves. However, the statistical information retrieved from 1000 different polymer simulations reveal much more interesting features of the system.

The results of generating 1000 different polymers of 1000 monomers each are presented in Figure 3. Probability Density Functions are plotted for the orientations, major radius, minor axis, and aspect ratio of the polymers. The orientations of the polymers are randomly distributed across the whole domain, as expected. The major and minor axis follow a gaussian distribution with peaks at 3.0 and 2.25, respectively. The distribution of the aspect ratio shows that all the values are above 1 and the peak lies at around 1.6. Moreover, we define the ratio of the average values of the radii as

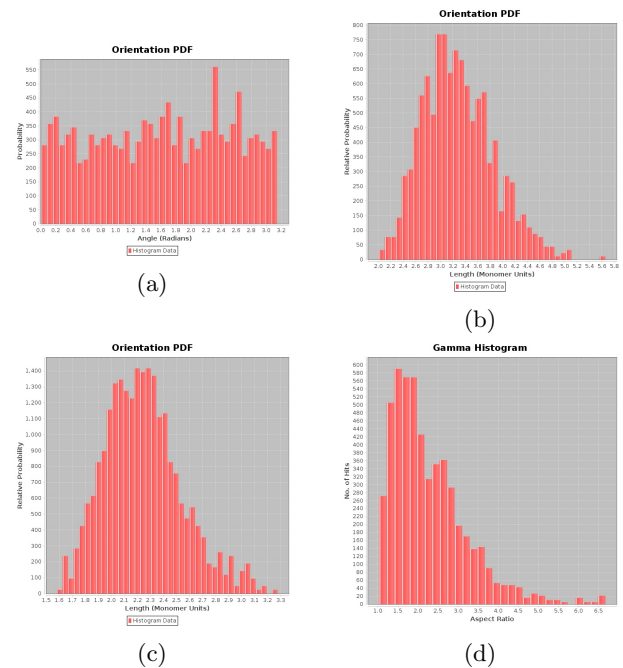


FIG. 3: The Probability density figures for the different parameters of the gaussian ellipse for 1000 different simulated polymers, each of 1000 monomers. (a) orientations of the polymers, (b) major radius of the ellipse α , (c) minor radius of the ellipse β , (d) aspect ratio of the polymer, defined as α/β

$$\gamma \equiv \langle \alpha_j \rangle / \langle \beta_j \rangle \quad (5)$$

and we find that $\gamma = 2.1$, which is approximately the same as the value of 2.2 reported by Haber et al.(1) This results show that the shapes of the polymers are mostly extended or elongated, with the orientations varying over the whole space. This shows a nonspherical symmetry of the system. The results of the computer simulations closely follow the results obtained in experiments studying flexible polymers in solutions through optical methods(1).

The results are consistent with the observations made by Haber et al. for the case where the polymers are 1000 monomers long(1). Here we also explore the different cases where the polymers have different lengths. We simulate polymers for 1000 different lengths, from $N = 1$ to $N = 1000$. We generate 1000 polymers for each N and plot $\langle R_{ee} \rangle$, $\langle R_g \rangle$, $\langle \alpha_j \rangle$, $\langle \beta_j \rangle$, and γ as functions of the polymers' length N .

The results from generating one million polymers show two interesting results. First, we see that the end-to-end radius, the gyration radius, and both of the radii from the gaussian ellipse follow the expected growth for diffusive motion. The end-to-end radius plot can be fitted to

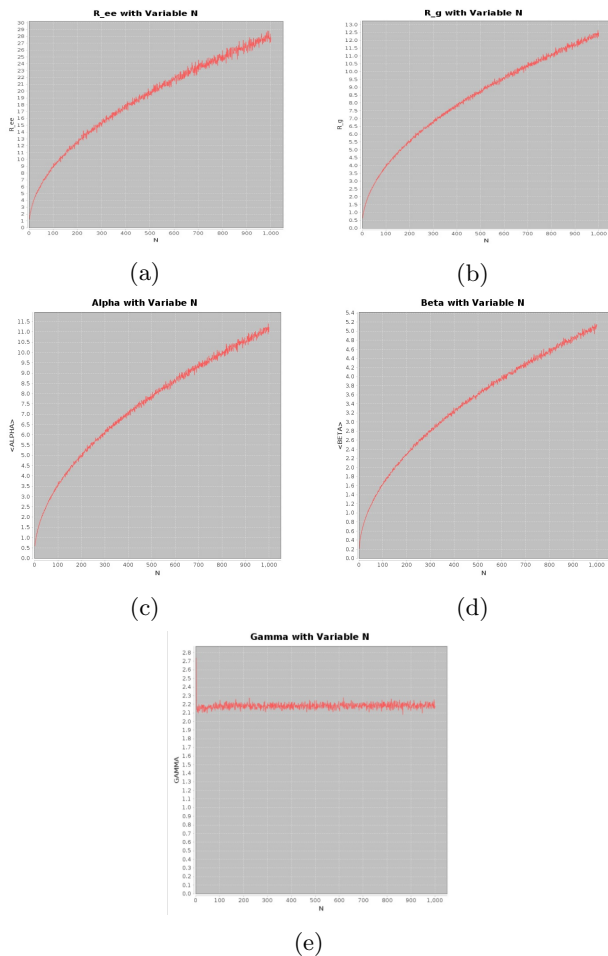


FIG. 4: Shape characterizations averaged over 1000 polymers and plotted as functions of the length N . (a) Average of end-to-end radius as a function of N , $\langle R_{ee} \rangle$, (b) average of gyration radius as a function of N , $\langle R_g \rangle$, (c) major radius of the ellipse $\langle \alpha \rangle$ as a function of N , (d) minor radius of the ellipse $\langle \beta \rangle$ as a function of N , (e) measurements of γ as a function of N .

$$R_{ee} \approx 0.95N^{0.49} \quad (6)$$

the gyration radius plot can be fitted to

$$R_g \approx 0.43N^{0.48} \quad (7)$$

the major radius of the ellipse to

$$0.39N^{0.48} \quad (8)$$

and the minor radius of the ellipse to

$$0.18N^{0.48} \quad (9)$$

This shows that all of these shape characterizations grow approximately as the square root of the number of steps taken, as expected in a diffusive motion system.

Second, the measurements of γ , $\langle \alpha_j \rangle / \langle \beta_j \rangle$, as a function of N , show almost a constant value around 2.18 showing a shape anisotropy for any flexible polymer independent of its length. The value measured by Haber et al. is approximately 2.2, which indicate a close relationship between our simulations and the T2-DNA chains used in their experiments.

CONCLUSIONS

The statistical information retrieved from the simulations reveals a very close relationship to real flexible polymers when compared to the results obtained by Haber et al. We conclude that there is a predominance of anisotropic polymer shapes and that this is due to the random walk nature of the polymers. Our simulations are purely mathematical and probabilistic, which suggest that the intramolecular interactions or any self-avoiding effects have little or no effect on the shapes or dynamics of flexible polymers. The shapes characterizations of our simulations follow closely the shape of DNA chains in solution and the accepted models for diffusive motion.

THE RANDOM WALK NATURE OF BROWNIAN MOTION

Now we explore Brownian motion and its relationship with a random walk. When we consider a system consisting of a spherical particle in a fluid, we think of the fluid as the sum of many small molecules (their size being much smaller than the size of the spherical particle) moving around. The little particles are constantly moving and colliding with the spherical particle. The result is the fluid constantly pushing the particle from seemingly random directions, leading to what is known as Brownian motion.

In our simulations we consider a spherical particle of radius a in water. As the water molecules move around and collide with the sphere a transfer of momentum occurs. If the change of momentum from one water molecule collision is $\Delta \mathbf{p}_i$, then the total change of momentum over a period of time where there occur N collisions is $\Delta \mathbf{P}_B = \sum_{i=1}^N \Delta \mathbf{p}_i$. Since we have the collisions coming from random directions, the average over many collisions should be $\langle \Delta \mathbf{P}_B \rangle \approx 0$, and the variance should be proportional to the number of collisions N , which is proportional to the product of the radius and the change of time. Hence, we have

$$\langle |\Delta \mathbf{P}_B|^2 \rangle = Aa\Delta t \quad (10)$$

and we define the transfer rate of the momentum as

$$\mathbf{f}_B \equiv \Delta \mathbf{P}_B / \Delta t \quad (11)$$

It is this transfer of momentum what we call a Brownian force, and as expected from all the random collisions, it is random.

However, the resulting motion of the spherical particle is not only due to the collision of water molecules and the Brownian force. As the particle is pushed through the liquid, more molecules hit the particle from one side than the other, in an anti-parallel fashion. This results in a drag force, \mathbf{f}_d , that we can calculate using Stoke's law.

$$\mathbf{f}_d \equiv \Delta \mathbf{P}_d / \Delta t = -\alpha \mathbf{v} \quad (12)$$

where α is equal to $6\pi\eta a$, and η is the viscosity of the liquid. When the Brownian force moves the particle in a particular direction, the drag force increases in an anti-parallel direction, the two forces are correlated, and we find that the constant A is equal to $2d(6\pi\eta)k_bT$, following Stoke's law and d is the system's dimension.

In our simulations we consider a particle trapped in a potential in a single dimension, resulting in Equation 13 as the equation of motion for the particle.

$$m \frac{dv}{dt} = -kx - 6\pi\eta av + \mathbf{f}_B \quad (13)$$

This is the Langevine equation and can be simplified further when the Renolds number is much less than 1. The resulting equation is

$$0 = -kx - 6\pi\eta av + \mathbf{f}_B \quad (14)$$

and if we integrate over a Δt we get

$$x(\Delta t) = Sx(0) + Bg \quad (15)$$

where $S = 1 - \frac{k\Delta t}{6\pi\eta a}$, $B = \sqrt{\frac{2k_bT\Delta t}{6\pi\eta a}}$, and g is a gaussian random number, hence $\langle g \rangle = 0$ and $\langle |g|^2 \rangle = 1$. For this particular system we will define the correlation function as

$$\langle x(t)x(t') \rangle = \frac{k_B T}{k} e^{-|\tau|/\tau_0} \quad (16)$$

Using Equation 15 we simulate the displacement of a one-dimensional particle at room temperature ($T \approx 300\text{K}$) and a spring constant of $k = 10\text{pN}/\mu\text{m}$.

The plot shows the particle rapidly falling from its initial position to its final position and fluctuates around

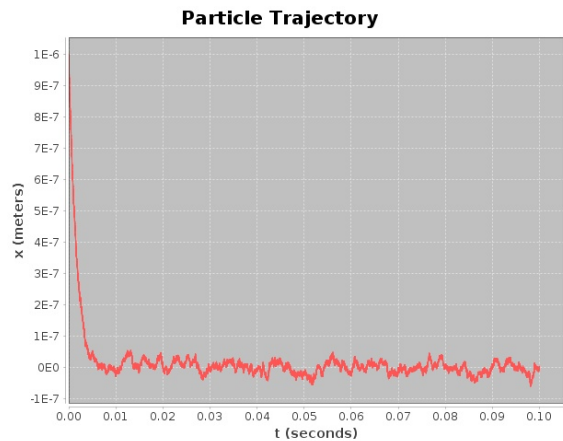


FIG. 5: Trajectory of a spherical particle in the x-axis. The particle is trapped in a potential and is at a room of 300K. The spring constant is $1 \times 10^{-5}\text{N/m}$.

the equilibrium point. However, in order to understand the rate of fluctuations within the system we define the fluctuation width as

$$w = 2\sqrt{\langle x^2 \rangle} \quad (17)$$

In order to interpret this measurement, we can compare the calculation to the value obtained from the correlation function for the system.

$$w = 2\sqrt{k_B T / k} \quad (18)$$

For the simulation plotted in Figure 5 the measured value is $w = 4.07 \times 10^{-8}\text{m}$ while the predicted value is $w = 4.04 \times 10^{-8}\text{m}$. This suggest that ignoring the inertia term in Equation 13 and ignoring any changes in the spring force due to small time intervals does not affect the predictions of the particle's trajectory. Moreover we extract the persistence time τ_0 from the correlation function and compare it to the predicted value,

$$\tau_0 = 6\pi\eta a / k \quad (19)$$

From the simulation we obtain that $\tau_0 = 0.00161$ while the predicted result is $\tau_0 = 0.00155$. For completeness, we plot new trajectories for different values of the spring constant and temperature. We then measure the fluctuation width and the persistence times as functions of spring constant k and temperature T .

The four plots from Figure 6 show that the stiffer the spring the faster the system settles at equilibrium and the less it fluctuates around this point. For increasing temperatures, the system reaches equilibrium faster but fluctuates more. The obtained and predicted values for the different plots are presented in the Table I.

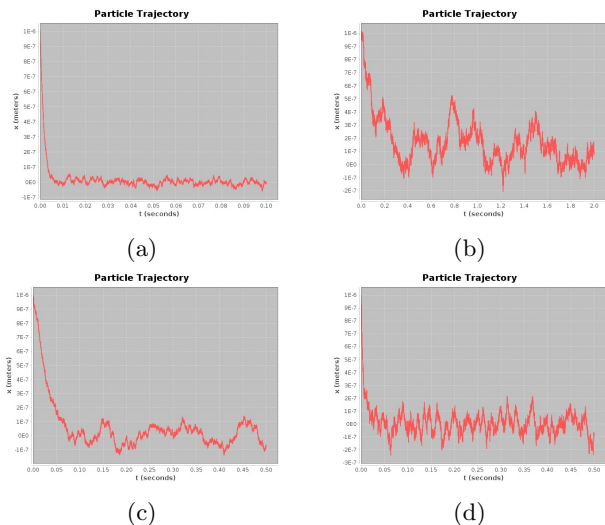


FIG. 6: Particle trajectories for different values of the spring constant and temperature of the system.

- (a) $k = 1.00 \times 10^{-5} \text{N/m}$ and $T = 300\text{K}$,
- (b) $k = 1.00 \times 10^{-7} \text{N/m}$ and $T = 300\text{K}$,
- (c) $k = 1.00 \times 10^{-6} \text{N/m}$ and $T = 273\text{K}$,
- (d) $k = 1.00 \times 10^{-6} \text{N/m}$ and $T = 373\text{K}$.

Moreover, after plotting the fluctuation width and the persistence time as functions of the spring constant and temperature, we find that both the fluctuation width and the persistence time decay rapidly when we change the spring constant, as shown in plots (a) and (c) of Figure 7, but the fluctuation width seems to slightly increase linearly as the temperature of the system increases, as shown in plot (d) of Figure 7.

Comparing to the predicted values, we find that when increasing the spring constant the obtained values are $T = 333.16\text{K}$ and $\eta = 9.45 \times 10^{-4} \text{Pa}\cdot\text{s}$, while the predicted values are 300K and $8.54 \times 10^{-4} \text{Pa}\cdot\text{s}$. In the case where we increase the temperature, we obtain a value

TABLE I: Observed and predicted values for the fluctuation width and the persistence time for the different values of k and T plotted in Figure 6.

Plot	Observed w	Predicted w
(a)	$4.04 \times 10^{-7} \text{m}$	$4.07 \times 10^{-7} \text{m}$
(b)	$4.12 \times 10^{-7} \text{m}$	$4.07 \times 10^{-7} \text{m}$
(c)	$1.35 \times 10^{-7} \text{m}$	$1.23 \times 10^{-7} \text{m}$
(d)	$1.39 \times 10^{-7} \text{m}$	$1.43 \times 10^{-7} \text{m}$
Plot	Observed τ_0	Predicted τ_0
(a)	0.00155s	0.00161s
(b)	0.167s	0.161s
(c)	0.0377s	0.0332s
(d)	0.00527s	0.00497s

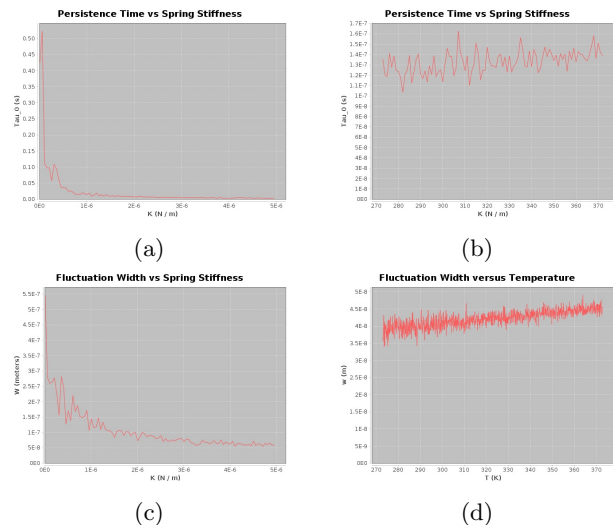


FIG. 7: Fluctuation width and persistence time as functions of the spring constant and temperature. (a) Persistence time as a function of spring constant, (b) zoom-in of plot (a) after the system has reached equilibrium, (c) fluctuation width as a function of spring constant, (d) fluctuation width as a function of temperature.

of $k = 1.35 \times 10^{-6} \text{N/m}$, while the predicted value is $1.00 \times 10^{-6} \text{N/m}$.

We now introduce a new mathematical tool, a Monte Carlo algorithm. The Langevine equation describes the trajectory of a particle as it reaches equilibrium, but we can use the Monte Carlo algorithm to study the equilibrium state of a particle in Brownian motion.

After reaching equilibrium with the Monte Carlo algorithm, a less expensive computation, we measure a value of $T = 318.19\text{K}$ while the predicted value was 300K for the case where we varied the spring constant, and measured a value of $k = 1.23 \times 10^{-6} \text{N/m}$ while the predicted value was $1.00 \times 10^{-6} \text{N/m}$ for the case where we varied the temperature.

CONCLUSIONS

We have explored a spherical particle in a one-dimensional fluid where the particle experiences an inertial force, a spring force, a Brownian force and a drag force, both due to the interaction with the surrounding water molecules. We have shown that we can safely disregard the inertial term and any change in the spring force and are able to approximately predict the trajectory of the particle using the Langevin equation. The results obtained from the simulations' measurements and the predictions obtained from the theory suggest that even though the Langevine provides more information regarding the transition towards equilibrium, the Monte Carlo

algorithm is computationally less expensive and predicts more accurately the distinct parameters of the system, such as the temperature and the spring constant, when the system has already achieved the equilibrium phase.

The results obtained for both flexible polymers and Brownian motion of particles in a one-dimensional medium using mathematical and probabilistic methods suggest that we can use our models to simulate and pre-

dict similar systems accurately, without having to synthesize and observe real physical systems.

REFERENCES

1. Haber, C., Ruiz, S. A., & Wirtz, D. (2000) PNAS (Princeton, NJ) **97**, 10792-10795.